COATINGSTECH CONFERENCE 2023

BEST PAPER AWARD

By Tahereh (Neda) Hayeri and Vijay Mannari, Ph.D., Coating Research Institute, Eastern Michigan University

Novel Versatile Oligomer for Thermally, UV-, and Ambient-Curable Organic-Inorganic Hybrid Coatings

"The organic-inorganic hybrid (OIH) system is one of the major products developed recently, especially for UV-curable coatings."

Editor's note: *A portion of this article was recognized with the Best Paper Award at the 2023 CoatingsTech Conference, held in Cleveland, OH, in June. The authors have since expanded the article with the addition of new data and updated information.*

1. Introduction

Binders are the essential ingredients in every coating formulation and primarily define the properties, applications, and curing technologies of the coating system. The most popular and commonly used binders in conventional coatings are usually designed to be cured by one specific curing technique, such as thermal curing, radiation curing, or ambient temperature curing. Systems with binders that can be cured with only one curing mechanism have inherent limitations, such as difficulty balancing hardness and flexibility, substrate characteristics, flow, leveling, and wettability, complete surface, through curing with no apparent defect, and poor adhesion to substrates in some cases. These shortcomings often require more application space.

UV-curable coatings are among the fastest growing systems due to their low energy input, rapid curing, and low- to zero-VOC compositions, making them sustainable alternatives. The most commonly used UV-curing processes are based on the free radical polymerization mechanism, which brings many challenges to the system, such as oxygen inhibition leading to an under-cured surface, volume shrinkage, and adhesion issues.[1] Some researchers have tried to overcome the challenges related to free radical systems mainly by replacing them with curing processes based on ionic polymerization. Cationic polymerization has been developed as a sustainable solution, as it is not sensitive to oxygen and benefits from full cure potential. However, besides limited availability and high price, cationic polymerization is also very sensitive to environmental humidity; although a small amount of water can be helpful for the reaction—as it can play a major role as a proton carrier and transfer agent—high humidity can inhibit the reaction and terminate the polymerization.[2] Systems using an anionic polymerization mechanism could be an option, as they have not been observed to have had this challenge, but their drawbacks include low quantum yields and relatively low basicity of the generated bases.[3]

Some efforts have been made to address the challenges related to the ionic system, such as using a humidity blocker approach, which involves adding a hydroxyl-functional reactive diluent and an epoxy siloxane; this combination creates a hydrophobic system that can block humidity.[4] Yet, taking full advantage of ionic polymerization requires a novel product. The organic-inorganic hybrid (OIH) system is one of the major products developed recently, especially for UV-curable coatings. The OIH system is based on a sol-gel reaction triggered by a strong acid or strong base catalyst. However, so many developments have been made in trying to initiate a sol-gel reaction by UV irradiation.

One such development is the synthesis of organosilanes containing epoxy and alkoxysilane functional groups and the use of photopolymerization, which uses photo acids and photo bases to cure.[5-8] Nayini et al. investigated the gel time and shrinkage of a UV-cured coating based on the OIH system. In their work, the organosilane oligomers have been synthesized based on tetraethoxysilane (TEOS) and tetraethylene glycol diacrylate. They used photo acids to initiate the sol-gel reaction after exposure under a UV mercury lamp. The results showed delayed gelation and reduced final film shrinkage as the portion of inorganic moieties increased in the formulation.[9] A review by Liu et al. discusses different preparation methods for OIH systems, including blending, sol-gel, intercalation polymerization, and in-situ reaction methods.[10] The authors' research group, Mannari et al., at the Coating Research Institute, Eastern Michigan University, has done extensive research in exploring UV-cure systems that can effectively address the aforementioned limitations inherent to free-radical and ionic polymerization mechanisms. They reported the development of OIH coatings that are cured by a UV-initiated sol-gel mechanism that is triggered by photo-latent catalysts. Specifically, they used coating compositions containing multi-functional organosilane precursors as oligomers and super photo-acid or photo-base catalysts to bring about a cure by sol-gel reaction using ambient moisture.[11-12]

Research using another approach yielded a system that can undergo the Michael-addition and sol-gel reaction upon UV exposure using a photo-base catalyst. The results indicated that a single UV trigger with tunable properties could easily cure a system like this by leveraging different cure reactions.[13] Asemani et al. compared photo acid and photo base generators to assess their use as catalysts for UV-initiated sol-gel curing systems, and the results showed that both super acid and super base catalysts could initiate the sol-gel reaction upon exposure to UV under ambient moisture.[14] In the authors' study, the team designed and synthesized

a family of a new generation of organosilane precursors.[15] They then added different catalysts based on the curing process. The team measured the FT-IR spectrum of the system before and after curing under various curing conditions: thermal, UV, ambient, and a combination of UV and ambient. They used the resulting FT-IR spectrum as a qualitative and quantitative method to find if multiple mechanisms could trigger the sol-gel reaction. Investigation of the properties of the cured coatings showed comparable characteristics when crosslinking started by different curing processes.

2. Materials and Method

2.1 Materials

Materials for the authors' study included 3 x 6 in. aluminum alloy (TRU Al) test panels (provided by ACT); Desmophen VPLS-2328, a polyester polyol with OH content = 8.0%, and Desmodur I, an isophorone diisocyanate (IPDI) monomer (both provided by Covestro AG); Dynasylan AMEO (3-aminopropyltriethoxy silane) was procured from Evonik Industries; and tetraethyl orthosilicate (TEOS) and xylene (both purchased from Sigma-Aldrich). The study also required three different catalysts: (1) Chivacure 1176, a photo-blocked diphenyl(4-phenylthio) phenylsulfonium hexafluoroantimonate and (thiodi-4,1-phenylene)bis(diphenylsulfonium) dihexafluoroantimonate (see **Figure 1**), provided by Chitec Technology Co., Taiwan; (2) K-Kat 670, a tin-free catalyst for ambient-curing of silane functional oligomers (provided by King Industries); and (3) CXC-1821, an antimony-free quaternary ammonium-blocked super acid catalyst for thermal curing (provided by King Industries).

FIGURE 1
The chemical structure of the Chivacure 1176 super acid catalyst.

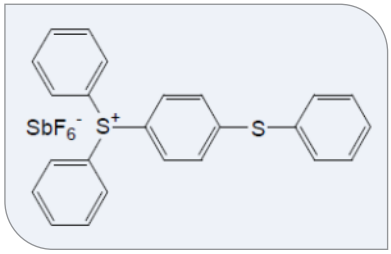

FIGURE 2
The chemical route to obtain the multifunctional silane precursor.

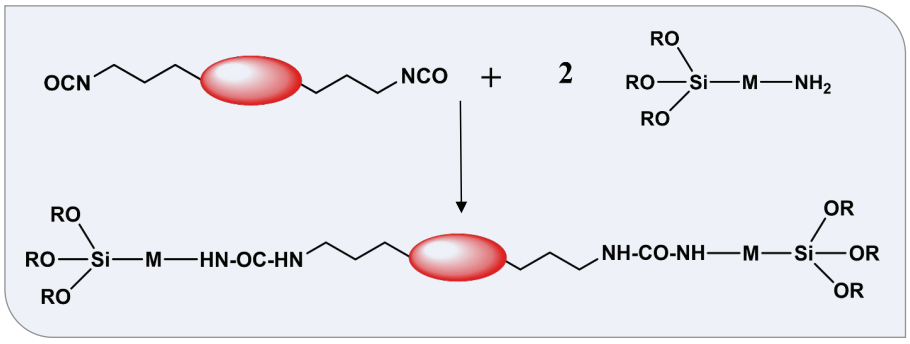

2.2 Methods

2.2.1 Synthesis of Isocyanate Prepolymer

During the first stage of synthesizing the isocyanate prepolymer, Desmophen VPLS-2328 was accurately measured and placed into a three-neck flask equipped with a mechanical stirrer, nitrogen inlet, temperature controller probe, and water condenser setup. The flask was heated to 80 °C, and once the desired temperature was reached and the contents were homogenized, IPDI was added dropwise from an addition funnel connected to a water condenser. Researchers recorded the starting time of the reaction and monitored the NCO content of the reaction hourly, following the ASTM D2572 method. Once the targeted level of NCO content was achieved after 4 hours, the heating was discontinued. Then, while the reaction mixture was gradually cooled to 70 °C, xylene was slowly added with continuous stirring. The amount of xylene added was 15 wt. % based on the total weight of the reaction mixture.

2.2.2 Synthesis of the Multifunctional Silane Precursor

The temperature of the prepolymer, prepared as described in section 2.2.1, was allowed to cool to a range of 20–30 °C. Subsequently, Dynasylan AMEO was slowly added from an addition funnel while the mixture was gently stirred. After a stirring duration of 30 minutes, the extent of the reaction was controlled by measuring the NCO content of the mixture, following the aforementioned ASTM method. The NCO value exhibited a decrease of 97% from its initial value, indicating the completion of the reaction between the NCO and amine. At this point, agitation was ceased, and the resulting product—the multifunctional silane precursor—was transferred to a plastic container and stored in a desiccator for further use.

Figure 2 shows the schematic of the chemical route to obtain the multifunctional silane precursor.

2.2.3 Preparation of Coating Compositions

Four different coating compositions were prepared by incorporating specific catalysts and TEOS as a reactive diluent. For the thermally curable coating, a 3% concentration of CXC-1821 catalyst was added based on the total solid content. In the case of the UV-curable coating, a 3% concentration of Chivacure 1176 catalyst was added based on the total solid content. The ambient-curable coating formulation included a 3% concentration of K-Kat 670 catalyst based on the total weight. Lastly, the dual-curable coating formulation consisted of a 3% concentration of Chivacure 1176 catalyst based on the total solid content and a 3% concentration of K-Kat 670 catalyst based on the total weight. All coating compositions were supplemented with 15% TEOS as a reactive diluent, serving to reduce the viscosity of the coating and enhance its applicability.

2.2.4 Curing Conditions

The curing processes that were employed for the four different coating types are as follows:

1. **UV-Curable Coating.** The UV-curable coating underwent four passes under a medium-pressure UV mercury H-bulb lamp on a Fusion UV-curing system. The lamp emitted UV radiation with an energy density of 0.7 j/cm^2, as measured by a compact radiometer (UVPS), while the conveyer speed belt was set to

operate at a rate of 13 feet/min. This exposure to UV radiation facilitated the photoinitiated curing process, leading to the desired crosslinking and solidification of the coating.

2. **Thermal-Curable Coating.** The thermal-curable coating was subjected to a controlled heating process for a duration of 20 minutes. An air-circulated oven was utilized to maintain a stable temperature of 90 °C. This elevated temperature triggered the sol-gel reaction, enabling the curing and crosslinking of the coating.

3. **Ambient-Curable Coating.** The ambient-curable coating was allowed to cure under ambient temperature and humidity conditions. No external heat or UV radiation was applied during this curing process. The natural ambient conditions provided the necessary environment for the gradual curing and crosslinking of the coating.

4. **Dual-Curable Coating.** The dual-curable coating followed a two-step curing process. Initially, the coating was exposed to UV radiation to initiate the photopolymerization reaction. Subsequently, the partially cured coating was allowed to further cure and crosslink under ambient conditions. This dual-curing approach offered the advantages of rapid initial curing with UV exposure, followed by extended curing to achieve optimal crosslinking and coating properties.

By tailoring the curing processes for each coating type, specific conditions were optimized to facilitate the desired chemical reactions and ensure the formation of a durable and well-cured coating film.

3. Results and Discussion

3.1 Characterization of the Multifunctional Silane Precursor by FT-IR

The synthesized oligomer was characterized using a Bruker-Tensor 27 FT-IR spectrometer, operating in the wavelength range of 4000 to 500 cm^{-1}, with KBr pellets as the sample medium. **Figure 3** illustrates the FT-IR spectrum obtained for the multifunctional silane precursor. Several distinctive peaks can be observed, each corresponding to specific molecular vibrations. The peak at 3337 cm^{-1} corresponds to the N-H stretching vibration of the urea linkage within the oligomer structure. The peaks observed at 2800–2900 cm^{-1} and 2957 cm^{-1} are assigned to the C-H stretching vibrations of methylene groups present in the oligomer. Additionally, a minor peak at 2260 cm^{-1} is attributed to the stretching vibration of residual NCO groups that might have remained from the synthetic process. Furthermore, prominent peak at 1720 cm^{-1}, indicating the carbonyl stretching vibration, suggests the successful formation of the urea linkage (-NH-CO-NH-) within the oligomer structure. Another notable peak observed at 1530 cm^{-1} further confirms the presence of the urea linkage. Additionally, the appearance of two distinct peaks at 1087 cm^{-1} and 950 cm^{-1} provides evidence for the presence of Si-O-R groups, which remained unchanged during the oligomer synthesis. The FT-IR characterization results provide valuable insights into the molecular structure and functional groups present in the synthesized oligomer. These insights support the oligomer's intended composition and provide a foundation for further analysis and application of the material.

3.2 Cure Study

3.2.1 FT-IR

The validation of the sol-gel reaction was conducted by monitoring the conversion of silane functional groups to siloxane linkages. This was achieved by observing the broadening peak in the FT-IR spectrum, which corresponds to the transition from the Si-O-C linkage to the Si-O-Si linkage within the range of 1050–1110 cm^{-1}.[16] The sol-gel reaction involves the transformation of alkoxysilane functional groups (-Si-OR) into siloxane (-Si-O-Si-) structures. The characteristic absorption peak of alkoxy silane groups (-Si-OR) appears sharp around 1080–1090 cm^{-1}, while the broadening of this peak within the range of 1050–1110 cm^{-1} signifies the formation of -Si-O-Si- structures. To confirm the occurrence and extent of the sol-gel reaction, the intensity and breadth of FT-IR peaks within the 1050–1110 cm^{-1} range were monitored before and after the curing process.

Additionally, to quantify the conversion of silane to siloxanes, the area under the Si-OR peak within the 1050–1110 cm^{-1} range was determined. The calculation was normalized using the reference peak at 1720 cm^{-1}, corresponding to the carbonyl bond, which is expected to remain constant throughout the crosslinking process. **Equation 1** was employed to compare

FIGURE 3
The FT-IR spectrum of the multifunctional silane precursor.

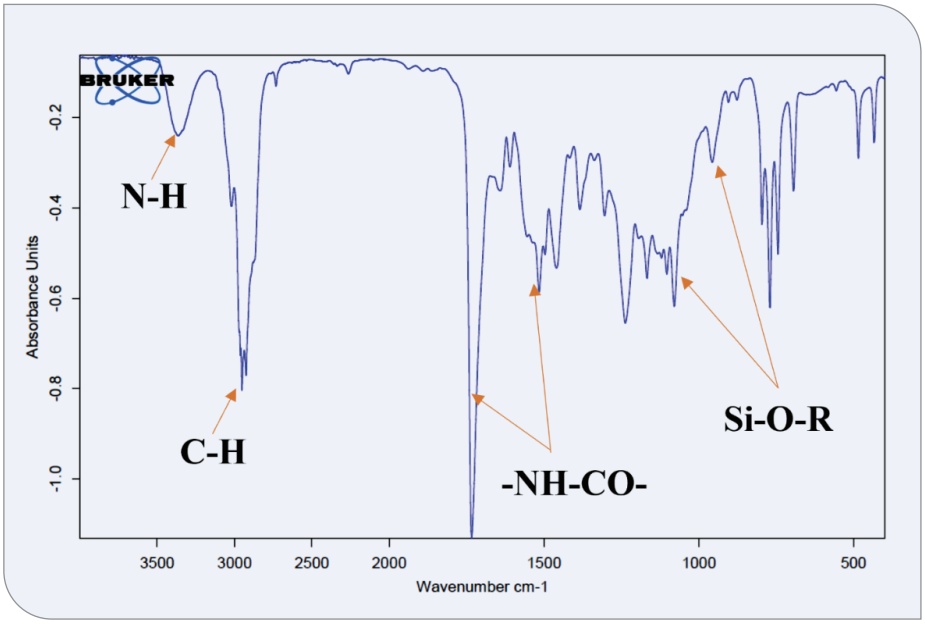

EQUATION 1

$$Conversion\ (\%) = 100 \times \frac{(A_{1087\ cm^{-1}}/A_{1720\ cm^{-1}})_{Cured}}{(A_{1087\ cm^{-1}}/A_{1720\ cm^{-1}})_{UnCured}}$$

the peak area of each coating before and after curing, enabling the calculation of the conversion percentage.[17]

The FT-IR samples were prepared by depositing a thin layer of each of the liquid coating compositions onto the surface of KBr pellets. Subsequently, IR spectra were recorded and designated as "before-curing" spectra. To examine the effects of curing, the same pellet was exposed to a UV source, and FT-IR spectra were re-recorded and labeled as "after-curing" spectra. This process was repeated for all the different coating compositions, utilizing various catalysts and employing multiple curing techniques. By systematically analyzing the before and after spectra for each coating composition, the changes and transformations that occurred during the curing process can be evaluated effectively.

Figure 4 illustrates the before-curing and after-curing FT-IR spectra for the thermally cured coating. Upon examination, significant changes in the peaks of interest following the curing process can be observed, which is indicative of a rapid reaction rate and a substantial transformation of Si-OR linkages to Si-O-Si linkages. The observed alterations in the spectral features provide compelling evidence for the efficiency of the thermal curing mechanism in facilitating the desired chemical conversions and the formation of the desired Si-O-Si linkages within the coating. Furthermore, the quantification of peak areas and subsequent calculation of the conversion percentage reveal a remarkable conversion efficiency of 87.4%. This quantitative analysis corroborates the successful progress of the thermal curing process and the substantial conversion of the Si-OR groups to the desired Si-O-Si structures within the coating matrix.

Figure 5 displays the "before-cure" and

FIGURE 4
Thermally curable coating before (red) and after (blue) curing in the oven (20 min at 90 °C).

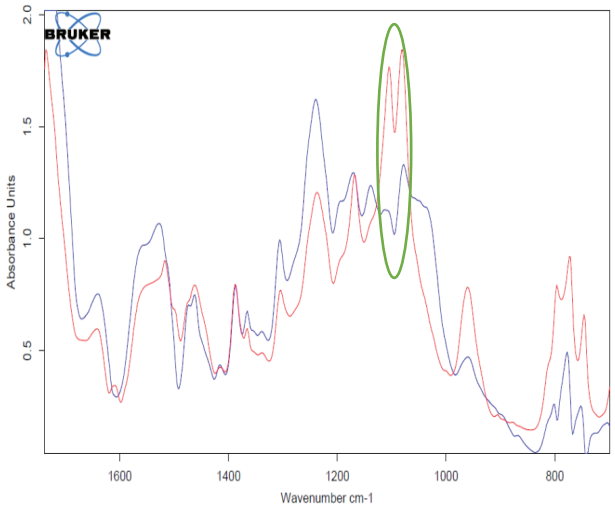

FIGURE 5
UV-curable coating before (red) and after (blue) curing under UV irradiation.

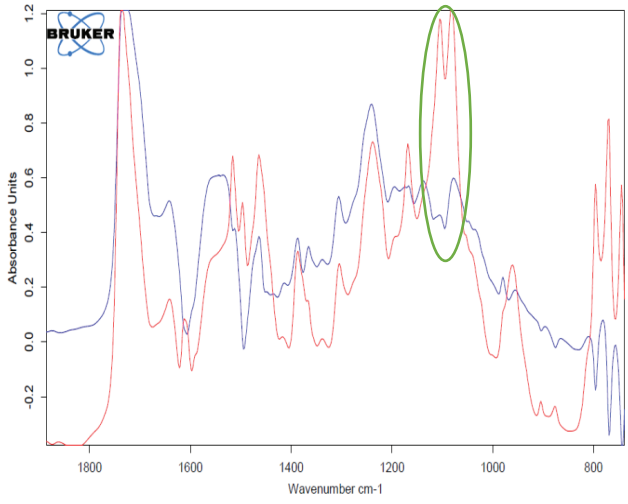

FIGURE 6
Ambient curable coating before (red), after 2 hours (green), and after 16 hours (pink) of curing under ambient conditions.

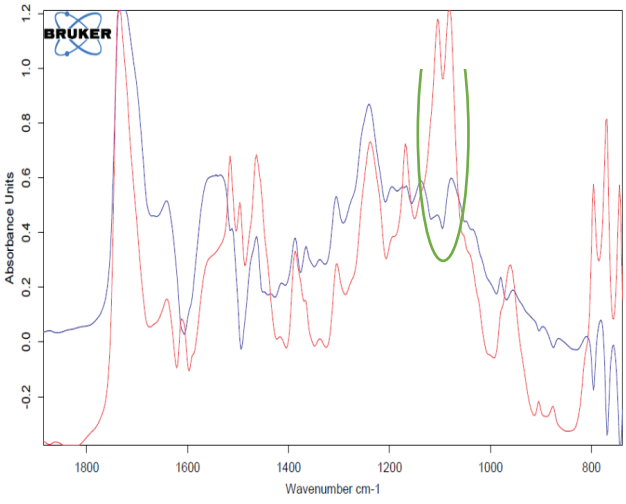

FIGURE 7
Dual-curable coating before (red), after exposure to UV (blue), and after 16 hours (pink) of curing under ambient conditions.

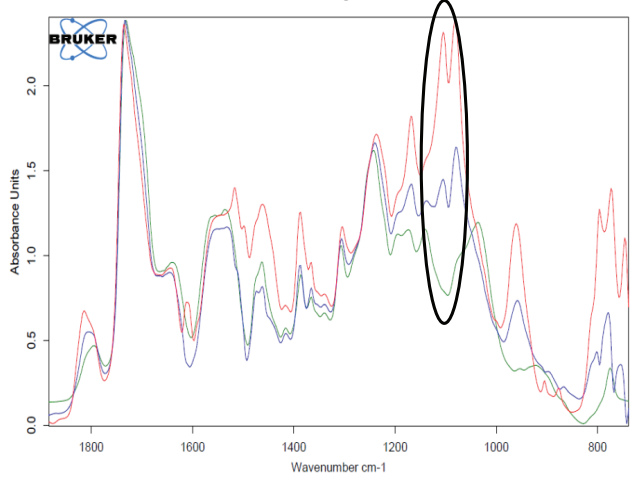

"after-cure" FT-IR spectra for the coating cured using UV radiation. Although the changes between the peaks of interest before and after curing are relatively minor compared with the peaks of the thermally cured coating, the observed broadening is still significant, indicating the conversion of Si-OR linkages to Si-O-Si groups upon exposure to the UV-mercury lamp. This broadening effect is an important indication of the crosslinking process occurring within the coating. Furthermore, the calculated conversion percentage calculated by the peak-area ratio method, which amounts to 79.9%, provides additional confirmation of the successful crosslinking that took place when the coated KBr pellets were subjected to UV radiation. This substantiates the efficacy of the UV-curing process in inducing the desired chemical transformations and the formation of Si-O-Si network within the coating matrix.

The curing behavior of the ambient-curable coating was found to be time-dependent. FT-IR spectra were recorded at various time intervals: before curing (right after the application of the wet film), after 2 hours, and after 16 hours of exposure to ambient conditions. Notably, a significant change in the spectra was observed, particularly after the 16-hour mark, as depicted in **Figure 6.** This demonstrates that the ambient-cure catalyst is capable of triggering the sol-gel reaction; however, achieving a tack-free film requires an extended period of time. This finding was further substantiated by calculating the conversion percentages, which were determined to be 58.2% after 2 hours and 73.5% after 16 hours. These results underscore the time-consuming nature of achieving a complete conversion and the development of a fully cured film in the case of the ambient-curable coating.

The behavior of the dual-curable coating, employing both UV and ambient-cure catalysts, exhibited distinct characteristics. **Figure 7** illustrates the FT-IR spectra, indicating an immediate and significant change in the peak of interest following UV exposure, signifying the activation of the UV catalyst and the initiation of the sol-gel reaction. Subsequently, FT-IR spectra were recorded after 16 hours of ambient exposure, revealing a notable broadening effect, indicative of an ongoing curing process. The dual-curing approach offers two notable advantages. Firstly, immediate formation of a complex and tack-free film occurs upon UV exposure, thereby presenting beneficial attributes for diverse applications. Secondly, areas not directly exposed to UV radiation can be cured using the ambient-cure catalyst, addressing challenges associated with shadow areas in the conventional UV-cure systems. For this specific coating composition, the calculated conversion percentages were found to be 69.5% and 81.5% immediately after UV exposure and after 16 hours of ambient exposure, respectively. These results provide strong evidence for the effectiveness of the dual-curing approach in achieving substantial conversion of the reactive components. Consequently, the dual-curable coating demonstrates the potential for the production of well-cured films with enhanced properties, both in terms of immediate curing and extended curing timeframes.

These results provide strong evidence for the effectiveness of the dual-curing approach in achieving substantial conversion of the reactive components.

3.2.2 Gravimetrical Analysis

Investigating the crosslinking density and cure extent represents a fundamental step in the analysis of various types of coatings. Hill et al. proposed multiple equations to quantitatively determine the crosslinking density in short-chain networks that involve a minimum of two reactive components.[18] Other researchers have proposed additional computational methods to predict the structure and properties of materials.[19,20]

In the context of a sol-gel system, the crosslinking process takes place through the hydrolysis of silane groups and results in the formation of silanol. Subsequently, the condensation of silanol and silane bonds leads to the creation of siloxane bonds. Throughout these reactions, a specific quantity of water and alcohol, proportional to the alkoxysilane content within the system is fully consumed, making the efficacy of the crosslinking process quantifiable. The cure extent can thus be determined by using the gravimetric method to measure the volatile loss of the system and calculating the theoretical weight loss based on the stoichiometric ratios of the reaction. **Equation 2** represents the principal sol-gel reaction responsible for the development of the crosslinking network in organic-inorganic hybrid coatings.

EQUATION 2

$$Si\text{-}OR + \tfrac{1}{2}\, H_2O = \tfrac{1}{2}\, Si\text{-}O\text{-}Si + ROH$$

To evaluate the extent of curing by using gravimetric monitoring via weight change, a series of oligomers with different molecular weights were synthesized and formulated by incorporating diverse catalysts. Subsequently, approximately one gram of each coating composition was deposited onto an aluminum dish, and the initial weight was recorded prior to the curing process. The appropriate technique to activate the reaction, corresponding to the specific catalyst utilized, was employed, and the weight was then re-recorded. The aluminum dishes, each containing a distinct coating, were left under ambient conditions, and their weights were recorded 16 hours and 168 hours (1 week) after the sol-gel reaction was initiated, which facilitated the formation of the organic-inorganic hybrid network via various techniques.

FIGURE 8
The gravimetric analysis of the cure extent of various coatings.

Analysis of Variance

Source	DF	Adj SS	Adj MS	F-Value	P-Value
Model	35	47118.2	1346.2	1797.31	0.000
Linear	7	44643.6	6377.7	8514.59	0.000
MW	2	552.7	276.3	368.91	0.000
Curing Catalyst	3	8344.3	2781.4	3713.38	0.000
Cure Schedule	2	35746.7	17873.4	23862.07	0.000
2-Way Interactions	16	2388.6	149.3	199.30	0.000
MW*Curing Catalyst	6	158.0	26.3	35.17	0.000
MW*Cure Schedule	4	33.6	8.4	11.21	0.000
Curing Catalyst*Cure Schedule	6	2196.9	366.2	488.84	0.000
3-Way Interactions	12	86.0	7.2	9.57	0.000
MW*Curing Catalyst*Cure Schedule	12	86.0	7.2	9.57	0.000
Error	36	27.0	0.7		
Total	71	47145.2			

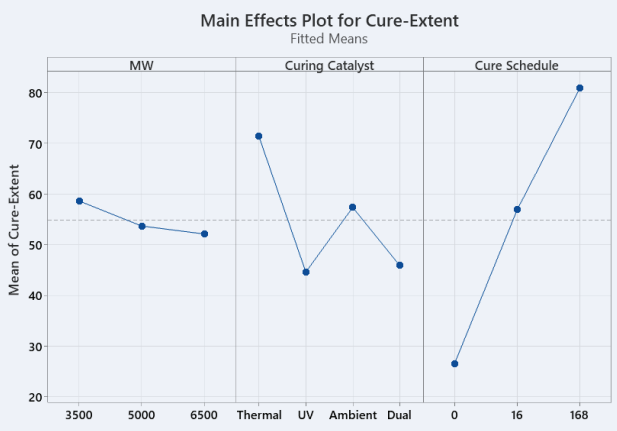

The collected data were analyzed with the design of experiment (DOE) method, implemented through Minitab software. **Figure 8** displays the results of the analysis of variance (ANOVA) table and the main effect plot, which provide insights into the statistical significance of the factors under investigation.

The results reveal a significant cure extent ($P<0.05$) across all coating compositions investigated. Also, as the molecular weight (MW) increases, a slight reduction in the cure extent was observed. This phenomenon could be attributed to a lower abundance of functional groups and a decrease in the concentration of active groups over time since the initiation of the reaction.

While all cure techniques exhibited a statistically significant cure extent, the thermally curable coating demonstrated the highest level of curing, aligning with expectations. In contrast, the UV- and dual-curable coatings displayed lower cure extents than anticipated. One potential explanation for this discrepancy is the occurrence of vitrification phenomena resulting from a high concentration of active groups, considering that both the oligomer and reactive diluent (TEOS) contain silane groups involved in the sol-gel reaction and crosslinking network. Addressing this issue may involve modifying the reactive diluent and optimizing the catalyst dosage. Ongoing research is currently exploring these avenues, and the outcomes will be presented in forthcoming studies.

FIGURE 9
Interaction plot of the gravimetric analysis of the cure extent for different coatings compositions.

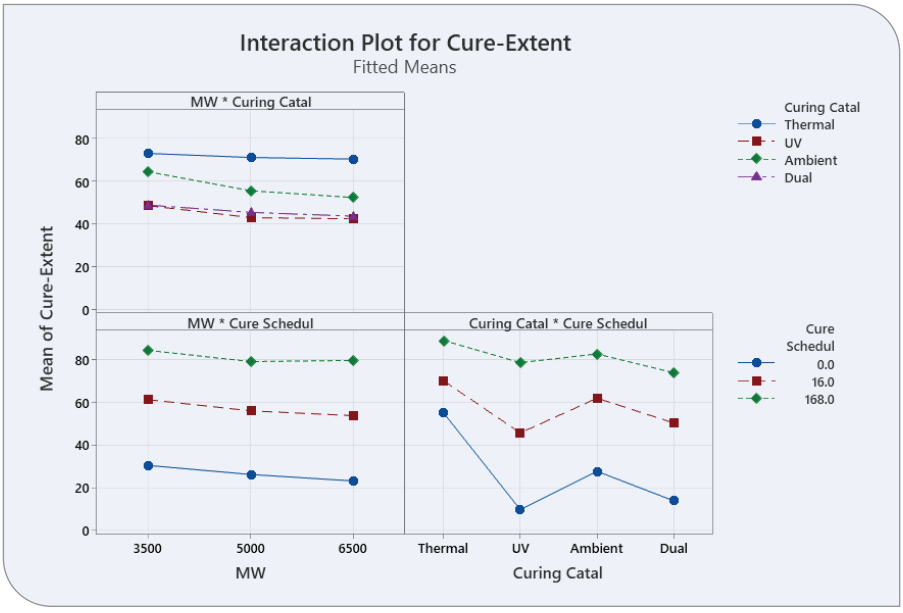

The main effect plot provides detailed insight into the curing behavior of the various coating compositions over time. It clearly demonstrates that the curing process continues to evolve as time progresses. This observation is further supported by **Figure 9**, which presents the interaction plot showcasing the cure extent of the different coatings. The plot provides a comprehensive representation of the dynamic nature of the curing process and highlights the changes in the extent of cure as a function of time for each coating composition. This scientific analysis emphasizes the ongoing and time-dependent nature of the curing process, reinforcing the notion that the coatings undergo progressive curing over the course of the experiment.

Table 1 shows the extent of cure obtained through FT-IR analysis using the peak-area ratio method and gravimetrical analysis using the weight-loss method. The extent of cure values represents the degree of crosslinking achieved for each coating composition, with higher values indicating a greater extent of cure.

The results show that the extent of cure for all the coating compositions exceeds

TABLE 1
Extent of Cure Obtained by FT-IR (Peak-Area Ratio Method) and Gravimetrical (Weight-Loss Method) Analysis

Cure Technique	Cure-Extent Using the "Peak-Area Ratio" Method (FT-IR)		Cure-Extent Using the "Weight-Loss" Method (Gravimetric)	
	0 hour	16 hours	0 hour	16 hours
Thermal	87.4 %	---	58.0 %	78.5 %
UV	79.9 %	---	15.8 %	52.5 %
Ambient	58.2 %	73.5%	31.9 %	60.0 %
Dual	69.5%	81.5%	19.8 %	54.6 %

50% after 16 hours, as determined by both the FT-IR (peak-area ratio method) and gravimetrical (weight-loss method) analyses. It is important to note that the observed difference in extent of cure values between the two methods can be attributed to the variation in coating thickness. In the FT-IR method, a thin layer of the coating was applied onto KBr pellets for analysis, resulting in a relatively uniform and controlled coating thickness. On the other hand, the gravimetrical method involved pouring approximately one gram of coating into aluminum dishes, where the thickness of the coating was not as uniform due to practical constraints. This variability in coating thickness led to a higher overall thickness in the gravimetrical method. Thus, the discrepancy in extent of cure values between the two methods can be attributed to the different coating thicknesses utilized. Despite this variation, both methods indicate that substantial curing had occurred within the 16-hour timeframe, with all coating compositions surpassing the 50% extent of cure threshold.

3.3 Properties of Cured Coatings

The aluminum test panels were coated with the different formulations utilizing a draw-down applicator, resulting in a precisely controlled wet film thickness of 2 mil (equivalent to 50 µm). The composition of each coating formulation was tailored in accordance with the type of catalyst employed, as previously described in section 2.2.4.

To comprehensively characterize the properties of the coatings, a rigorous assessment was conducted following the relevant ASTM standards. The MEK double rub test, based on ASTM D4752-20, was performed to evaluate the resistance of the coatings to solvent-induced rubs and thus provide an indication of their crosslinking density. The König pendulum hardness test, determined in accordance with ASTM D4366-21, was utilized as a quantitative measure of coating hardness. The cross-cut adhesion test, following ASTM D3359-23, was employed to assess the ability of the coatings to adhere firmly to the substrate, and it involved creating precise incisions and evaluating the extent of coating detachment. Specular gloss was determined using standard ASTM D523-18.

To comprehensively characterize the properties of the coatings, a rigorous assessment was conducted following the relevant ASTM standards.

Throughout the course of the sol-gel reaction, the MEK double rub test and König pendulum hardness test measurements were performed at specific time intervals: immediately after the initiation of the reaction (0 hours), after 16 hours, and following one week of the reaction, representing key stages in the progression of the crosslinking process. This time-resolved approach facilitated the investigation of the temporal evolution of the coating properties, allowing for a detailed examination of changes in mechanical resistance and performance characteristics as the sol-gel reaction advanced and the coatings underwent crosslinking.

The analysis of the results revealed that the thermally curable coating showed minimal variation in properties over time. This finding suggests that the extent of curing did not significantly increase beyond the point when the panels were removed from the oven. In other words, the curing process reached a plateau, indicating a high level of completion. The UV-curable coating showed no substantial change in properties between the initial measurement at 0 hours and the assessment conducted after 16 hours. However, a significant increase in properties was observed after 168 hours (1 week). This finding indicates that the UV-curing process continued to progress and reach higher levels of cure over an extended period of time. In the case of both the ambient- and dual-curable coatings, the results exhibited a notable change in properties from the initial measurement at 0 hours to the assessment conducted after 16 hours. Furthermore, after one week, another considerable change in properties was observed. These findings suggest that, for these coatings, the curing process continued to advance and evolve significantly even beyond the initial 16-hour period. Overall, these findings indicate that the curing behavior and the time required for optimal cure differ among the various coating formulations and cure schedules. These observations highlight the importance of considering the specific curing characteristics and time-dependent properties when assessing the performance and suitability of different coatings for specific applications.

The coatings containing the thermally blocked super acid catalyst exhibited a higher number of MEK double rub test cycles, indicating a greater extent of conversion of alkoxysilane functional groups (-Si-OR) into siloxane (-Si-O-Si-) structures when triggered by the thermal-curing technique. This finding was further supported by the FT-IR spectrum analysis that was performed before and after curing, as shown in **Figure 4**. The results of the MEK double rub test for the UV-curable coating also indicated a high level of crosslinking density within the fully cured, tack-free film. In contrast, the coatings utilizing the ambient-cure catalyst and a combination of the ambient and UV catalysts demonstrated

GRAPH 1
The results of the MEK double rub test for coatings with various cure catalysts.

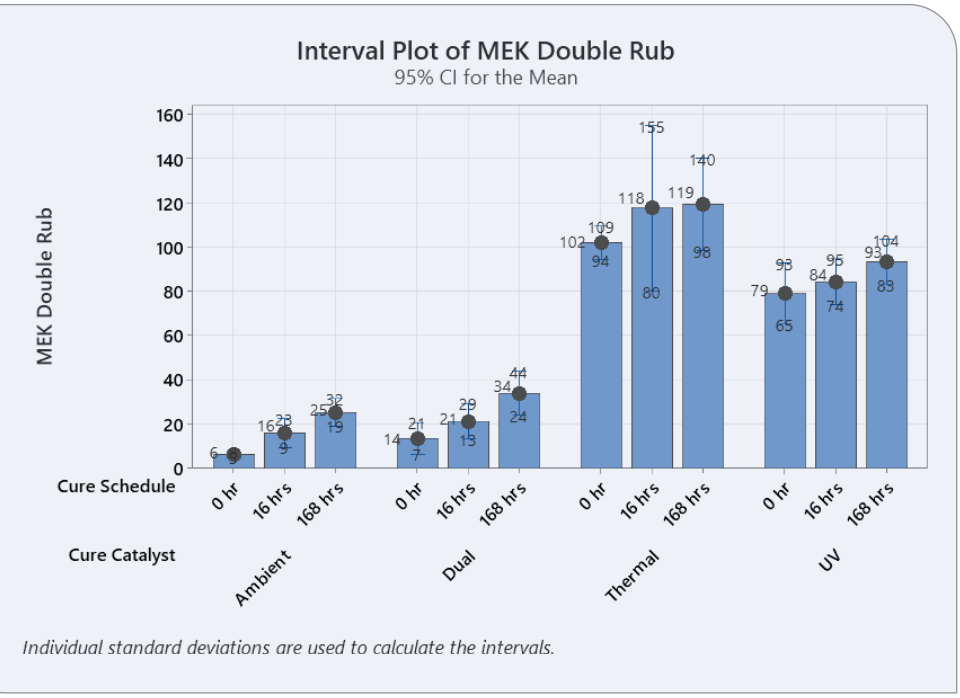

Individual standard deviations are used to calculate the intervals.

GRAPH 2
The results of the König pendulum hardness test for coatings with various cure catalysts.

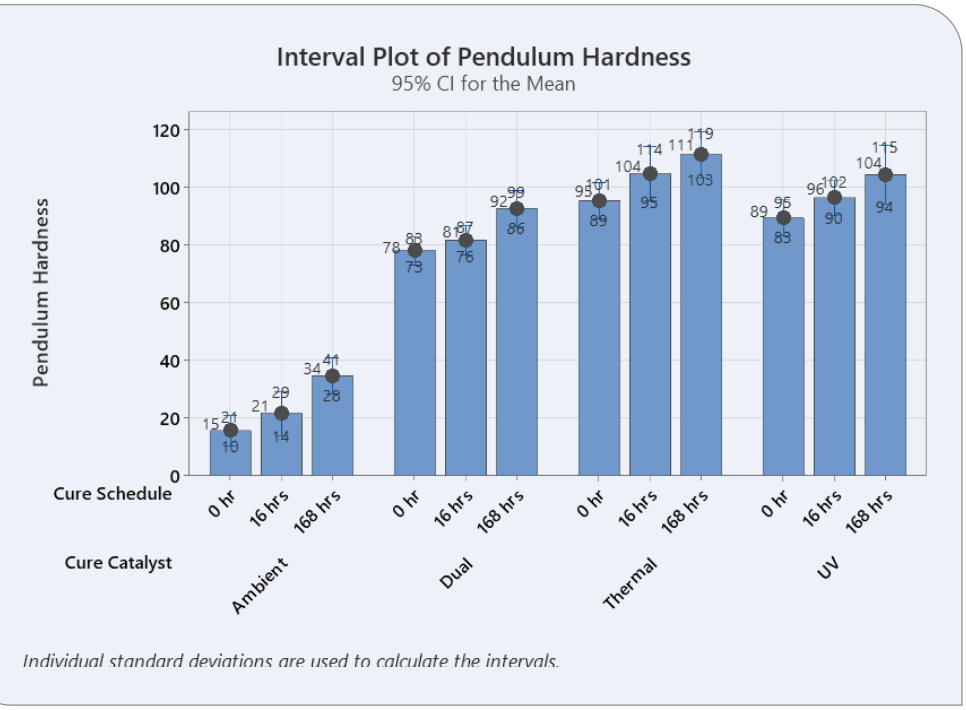

Individual standard deviations are used to calculate the intervals.

lower MEK double rub test results, suggesting that a longer period of time is required for the sol-gel reaction to expand and achieve a higher level of crosslinking density. However, it is worth noting that, overall, the MEK double rub test results for all coating compositions remained below 200, which is considered unacceptable for many application scenarios. One possible explanation for this observation is the trapping of TEOS molecules between the oligomer chains and the organic-inorganic hybrid network, resulting in their incomplete reaction. These unreacted TEOS molecules may be susceptible to MEK attack, leading to a decrease in the number of cycles and causing softening or damage to the coating. Ongoing research is focused on addressing these challenges, and the outcomes will be published in future works. This ongoing work aims to further investigate and understand the underlying mechanisms that impact the MEK double rub test results and to develop strategies for improving the performance and applicability of the coatings in various applications.

While there was a notable difference observed in the MEK double rub test results among the various coating compositions, the König pendulum hardness measurements showed a less significant variation for the thermal-, UV-, and dual-curable coatings. This finding suggests that the surface curing of these three coating compositions is sufficiently extended, providing them with appropriate hardness and suitability for a range of applications. However, the König pendulum hardness results for the coating with the ambient-cure catalyst indicated that this particular composition is relatively softer compared with the others. This lower hardness rating may limit the number of possible applications for this specific coating composition, as the result means it may be more susceptible to scratches and wear. To provide a visual representation of these results, **Graph 1** illustrates the MEK double rub test results, while **Graph 2** depicts the König pendulum hardness measurements.

The visual appearance of the various coating compositions was assessed by measuring the specular gloss at a 60° angle using a BKY gloss meter. The panels were placed under ambient conditions for 16

hours after curing, and then the gloss measurements were taken. The results demonstrated that all the coatings exhibited a high gloss appearance, with gloss values exceeding 80 in the 60° angle measurement.

However, it was observed that the thermal- and UV-curable coatings displayed higher gloss levels, as expected due to their higher crosslinking density. This outcome aligns with the notion that a greater degree of crosslinking leads to improved surface smoothness and enhanced glossiness. **Graph 3** illustrates the gloss measurements obtained for the different coating compositions.

To evaluate the adhesion properties of the coated panels, a crosscut test was conducted after one week. The test panels were subjected to the crosscut method, and the adhesion was assessed based on the ASTM chart, as depicted in **Figure 10**.[21] The results indicated that all the coated panels exhibited excellent adhesion, as they achieved a grade of 5B, according to the ASTM adhesion rating scale. This rating signifies that no peeling or detachment of the coating was observed during the crosscut test. The absence of peeling indicates strong adhesion between the coating and the substrate, highlighting the effectiveness of the coating formulations in promoting durable and reliable adhesion. These findings demonstrate the robust adhesion properties of the tested coatings and further validate their suitability for various applications where adhesion strength is a critical requirement.

4. Conclusion

The findings of this study highlight the exceptional adaptability of the new generation of precursors when combined with diverse catalysts. This adaptability greatly facilitates the initiation of the sol-gel reaction using different curing techniques within the developed system. The observed significant differences in the conversion of Si-O-R linkages to Si-O-Si linkages immediately after curing for coatings with thermal and photolabile catalysts, as well as coatings with the ambient-cure catalyst, highlight the distinct behavior of these formulations. However, it can be concluded that the crosslinking process can be effectively

GRAPH 3
The results of the specular gloss at 60° for coatings with various cure catalysts.

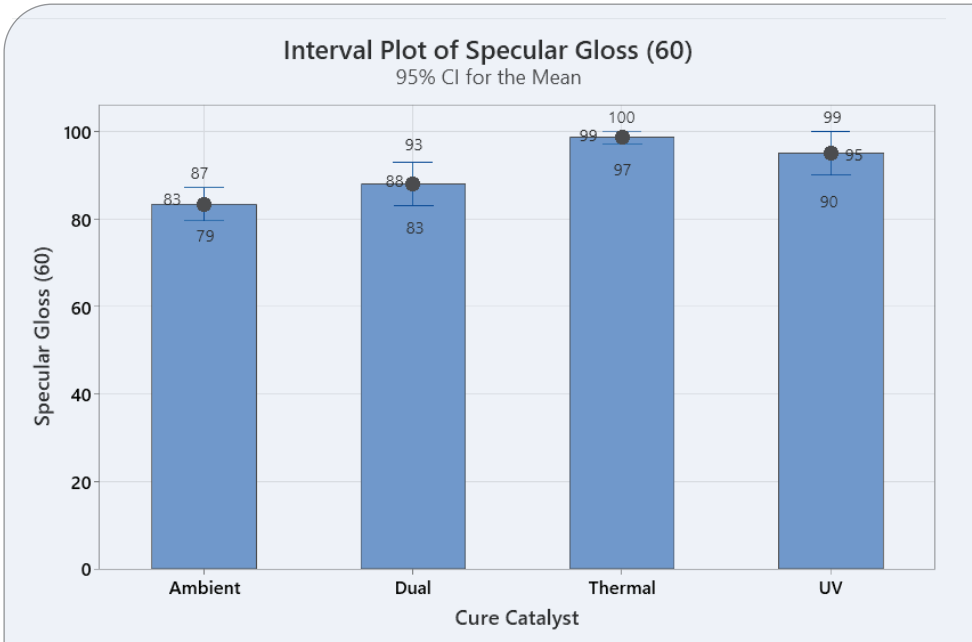

Individual standard deviations are used to calculate the intervals.

FIGURE 10
ASTM chart for grading the crosscut adhesion test.

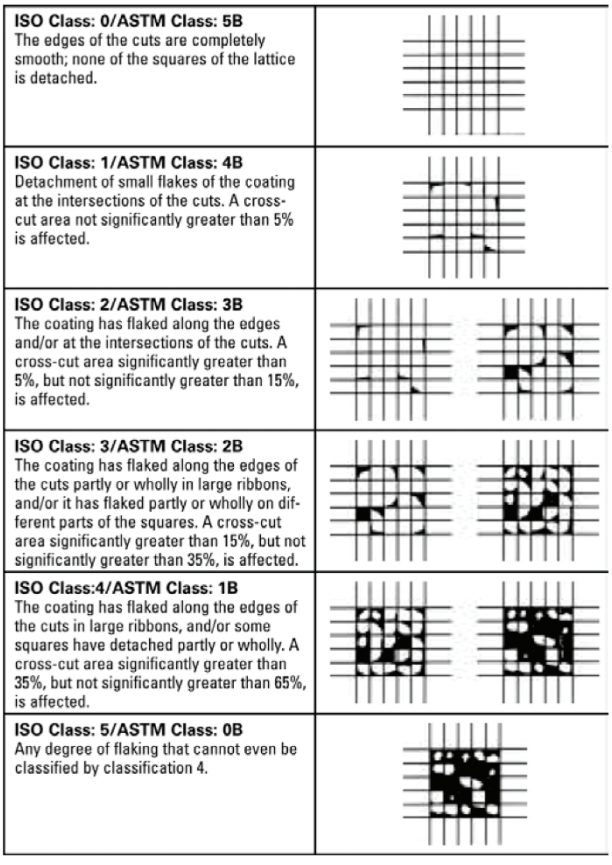

triggered using multiple curing techniques. In addition, the developed system demonstrates improved versatility by incorporating a dual-curable coating system that effectively combines both UV- and ambient-cure catalysts. This combination, along with its compatibility with other curing techniques, adds significant value to the system's flexibility and functionality. This research shows the potential for more innovative applications, such as dark-curing processes. The authors' research group, Mannari et al., has been actively investigating the optimization of ingredients, curing conditions, and other variables within these coating systems to identify the most suitable application for each curing technique. Additionally, the formulation of these coatings as high solid coatings (85% in xylene) eliminates the need for conventional acrylate reactive diluents, thereby reducing the presence of hazardous materials and enhancing the overall sustainability profile of the resulting new-generation coatings.

Further research is underway to address the observed challenges related to crosslinking and coating properties. Additionally, future efforts will be focused on reducing the VOC levels in the final product, thus contributing to environmental sustainability. ❊

Acknowledgments

The authors of this paper wish to thank all the suppliers that have provided the samples in the shortest possible time.

Tahereh (Neda) Hayeri is a Ph.D. candidate at Coatings Research Institute, GameAbove College of Engineering and Technology, at Eastern Michigan University. Email: thaeri@emich.edu. Vijay Mannari, Ph.D., is professor and director at the Coatings Research Institute. Email: vmannari@emich.edu.

References

1. Wicks, Z. W., Jr.; Jones, F. N.; Pappas, S. P.; Wicks, D. A. Radiation Cure Coatings. In *Organic Coatings*; Wicks, Z. W., Jr., Jones, F. N., Pappas, S. P., Wicks, D. A., Eds.; John Wiley & Sons: New Jersey, 2007; pp 574-594.
2. Maurin, V.; Bano, G. "How Cationic Curing can be a sustainable solution for challenging applications." Radtech Conference 2022, May 2022; https://www.radtech2022.com/wp-content/uploads/2022/05/1B-Engberg.pdf (accessed July 25, 2023).
3. Nobuhiro, I.; Koji, A.; Masahiro, F.; Takahiro, G.; Yoshimoto, A. "Photosensitivity Characteristics of UV Curable Organic-Inorganic Hybrids Sensitized with Benzoin Derivatives as Photobase Generators." *J. Photopolym. Sci. Technol.* 2014, 27 (2), 223-225. https://doi.org/10.2494/photopolymer.27.223.
4. Chen, Z.; Zhang, Y.; Chisholm, B.; Webster, D. "A humidity blocker approach to overcoming the humidity interference with cationic photopolymerization." *J. Polym. Sci.*, Part A: Polym. Chem. 2008, 46, 4344-4351. https://doi.org/10.1002/pola.22754.
5. Chemtob, A.; Versace, D.-L.; Belon, C.; Croutxé-Barghorn, C.; Rigolet, S. "Concomitant Organic–Inorganic UV-Curing Catalyzed by Photoacids." *Macromolecules* 2008, 41 (20), 7390-7398. https://doi.org/10.1021/ma801017k.
6. Versace, D.-L.; Chemtob, A.; Croutxé-Barghorn, C.; Rigolet, S. "Synthesis of Organosilica Films Through Consecutive Sol/Gel Process and Cationic Photopolymerization." *Macromol. Mater. Eng.* 2010, 295, 355-365. https://doi.org/10.1002/mame.200900318.
7. Chemtob, A.; Ni, L.; Croutxé-Barghorn, C.; Boury, B. "Ordered Hybrids from Template Free Organosilane Self-Assembly." *Chem. Eur. J.* 2014, 20, 1790-1806. https://doi.org/10.1002/chem.201303070.
8. Chemtob, A.; Courtecuisse, F.; Croutxé-Barghorn, C.; Rigolet, S. "Simultaneous sol-gel and anionic photopolymerization of 3-(glycidyloxypropyl) trimethoxysilane via photo base catalysis." *New J. Chem*. 2011, 35 (9), 1803-1808. https://doi.org/10.1039/C1NJ20320G.
9. Raei Nayinia, M. M.; Bastani, S.; Moradian, S.; Croutxe-Barghorn, C.; Allonas, X. "Rheological Investigation of the Gel Time and Shrinkage in Hybrid Organic/inorganic UV Curable Films." *J. Photopolym. Sci. Technol.* 2016, 29 (1), 105-110. https://doi.org/10.2494/photopolymer.29.105.
10. Liu, F.; Liu, A.; Tao, W.; Yang, Y. "Preparation of UV curable organic/inorganic hybrid coatings-a review." *Prog. Org. Coat*. 2020, 145, 105685. https://doi.org/10.1016/j.porgcoat.2020.105685.
11. Mannari, V. et al. U.S. Patent 11,414,524, August 16, 2022. Assignee: Eastern Michigan University, USA.
12. Mannari, V.; Hayeri, T. (N.); Asemani, H. "UV-initiated Organic-Inorganic Hybrid coatings for Advanced & Sustainable Applications." In Proceedings of Radtech, BigIdeas Conference 2023; July 2023; Available at: https://www.dropbox.com/scl/fo/58jvr25pw84god09vmlc5/h/MANNARI%20-%20UV-initiated%20deposition.pdf?dl=0&rlkey=puni5k6gqnn5n6zouuofnqo4i (accessed July 25, 2023).
13. Manchanda, H.; Mannari, V. "Super photo-base initiated organic-inorganic hybrid coatings by plural-cure mechanisms." *Prog. Org. Coat.* 2019, 127, 222-230. https://doi.org/10.1016/j.porgcoat.2018.11.011.
14. Asemani, H. R.; Luo, L.; Mannari, V. "Corrosion-resistant organic-inorganic hybrid pretreatments obtained by UV-initiated process suitable for primer-less coating systems." *Prog. Org. Coat.* 2020, 147, 105878. https://doi.org/10.1016/j.porgcoat.2020.105878.
15. Hayeri, T. (N.); Mannari, V. "UV-Enabled Moisture-Curing Systems: Novel Family of Versatile Oligomers for Expanding Application Space." In Proceedings of Radtech, BigIdeas Conference 2023; July 2023; Available at: https://www.dropbox.com/scl/fo/58jvr25pw84god09vmlc5/h?dl=0&preview=HAYERI+-+OIH+dual+-curable+system.pdf&rlkey=puni5k6gqnn5n6zouuofnqo4i (accessed July 25, 2023).
16. Coates, J. "Interpretation of Infrared Spectra, A Practical Approach." In *Interpretation of Infrared Spectra, A Practical Approach*; Meyers, R., Ed.; John Wiley & Sons Ltd: Chichester, 2000; pp 10815-10837.
17. Zareanshahraki, F.; Mannari, V. "'Green' UV-LED gel nail polishes from bio-based materials." *Int. J. Cosmet. Sci*. 2018, 40, 555-564. https://doi.org/10.1111/ics.12497.
18. Hill, L. W. "Calculation of crosslink density in short-chain networks." *Prog. Org. Coat.* 1997, 31 (3), 235-243. https://doi.org/10.1016/S0300-9440(97)00081-7.
19. Bazmara, M.; Silani, M.; Dayyani, I. "Effect of functionally-graded interphase on the elastoplastic behavior of nylon-6/clay nanocomposites; a numerical study." *Defence Technol*. 2021, 17 (1), 177-184. https://doi.org/10.1016/j.dt.2020.03.003.
20. Bazmara, M.; Silani, M.; Mianroodi, M.; Sheibanian, M. "Physics-informed neural networks for nonlinear bending of the 3D functionally graded beam." *Structures* 2023, 49, 152-162. https://doi.org/10.1016/j.istruc.2023.01.115.
21. DeFelsko Inspection Instruments website. https://www.defelsko.com/resources/finish-coatings-system-adhesion-and-test-methods (accessed July 25, 2023).